

Topologically-protected single-photon sources in topological slow light photonic crystal waveguides

Kazuhiro Kuruma,^{1, 2, 3,*} Hironobu Yoshimi,^{1,2} Yasutomo Ota,^{4,5} Ryota Katsumi,^{1,2}
Masahiro Kakuda,⁵ Yasuhiko Arakawa,⁵ and Satoshi Iwamoto^{1,2,5}

¹ *Research Center for Advanced Science and Technology, The University of Tokyo, 4-6-Komaba, Meguro-ku, Tokyo 153-8505, Japan*

² *Institute of Industrial Science, The University of Tokyo, 4-6-1 Komaba, Meguro-ku, Tokyo 153-8505, Japan*

³ *John A. Paulson School of Engineering and Applied Sciences, Harvard University, Cambridge, MA 02138, USA*

⁴ *Department of Applied Physics and Physico-Informatics, Keio University, 3-14-1 Hiyoshi, Kohoku-ku, Yokohama, Kanagawa 223-8522, Japan*

⁵ *Institute of Nano Quantum Information Electronics, The University of Tokyo, 4-6-1 Komaba, Meguro-ku, Tokyo 153-8505, Japan*

*Corresponding author: kuruma@iis.u-tokyo.ac.jp

Abstract

Slow light waveguides are advantageous for implementing high-performance single-photon sources required for scalable operation of integrated quantum photonic circuits (IQPCs), though such waveguides are known to suffer from propagation loss due to backscattering. A way to overcome the drawback is to use topological photonics, in which robust waveguiding in topologically-protected optical modes has recently been demonstrated. Here, we report single-photon sources using single quantum dots (QDs) embedded in topological slow light waveguides based on valley photonic crystals. We observe Purcell-enhanced single-photon emission from a QD into a topological slow light mode with a group index over 20 and its robust propagation even under the presence of sharp bends. These results pave the way for the realization of robust and high-performance single-photon sources indispensable for IQPCs.

High-performance single-photon sources are recognized as a key element for scalable operation of integrated quantum photonic circuits (IQPCs) based on discrete variables. To implement such a quantum light source, it is essential to incorporate solid-state quantum emitters, such as semiconductor quantum dots (QDs), into photonic nanostructures for efficiently funneling their radiation into IQPCs. Among various platforms, slow light waveguides in photonic crystals (PhCs) [1] are particularly attractive. The slow light modes largely enhance light-matter interactions, which accelerate the emission of quantum emitters into the modes via the Purcell effect and thereby boost the performance of the single-photon source. In addition, the photonic bandgap effect in the PhCs strongly suppresses unwanted radiation into non-guided modes and thus further improves the source efficiency. Importantly, the slow light waveguides in PhCs have also been employed for studying nonlinear optics at single-photon levels [2], and chiral light-matter interactions [3]. However, PhC waveguides are known to often suffer from non-negligible propagation loss due to backscattering, which becomes more prominent when approaching the slow light regime [4,5]. Since the backscattering is induced by structural imperfections, which are inevitably accompanied with nanofabrication processes, a rather different approach might be necessary to solve the issue.

One possible strategy for mitigating the scattering loss in the slow light PhC waveguides is the use of topological photonics. Topologically-protected modes have been demonstrated to exhibit robust waveguiding immune to disorders [6]. Among reported topological waveguides, those based on valley photonic crystals (VPhCs) [7–14] have attracted much attention, since they can be realized using simple dielectric slabs. Therefore, VPhCs can be naturally implemented in conventional photonic integrated circuit platforms [7,8] and hence can be combined with QDs [9,11,15,16]. So far, the coupling of single QDs to topological waveguides have been demonstrated [17]. However, all these demonstrations utilized fast light modes that naturally emerge in topological bandgaps. In contrast to slow light modes, such fast light modes could exhibit only moderate enhancement in light-matter interactions.

In this Letter, we report single-photon sources based on single QDs embedded in topological slow light VPhC waveguides. Single QDs coupled to the topological slow light waveguide exhibit large Purcell enhancement of spontaneous emission rate up to a factor of ~ 12 . The generated single-photons robustly propagate through the slow light mode with a high group index (n_g) over 20 even with sharp waveguide bends. These results pave the way toward high-performance integrated quantum light sources required for IQPCs.

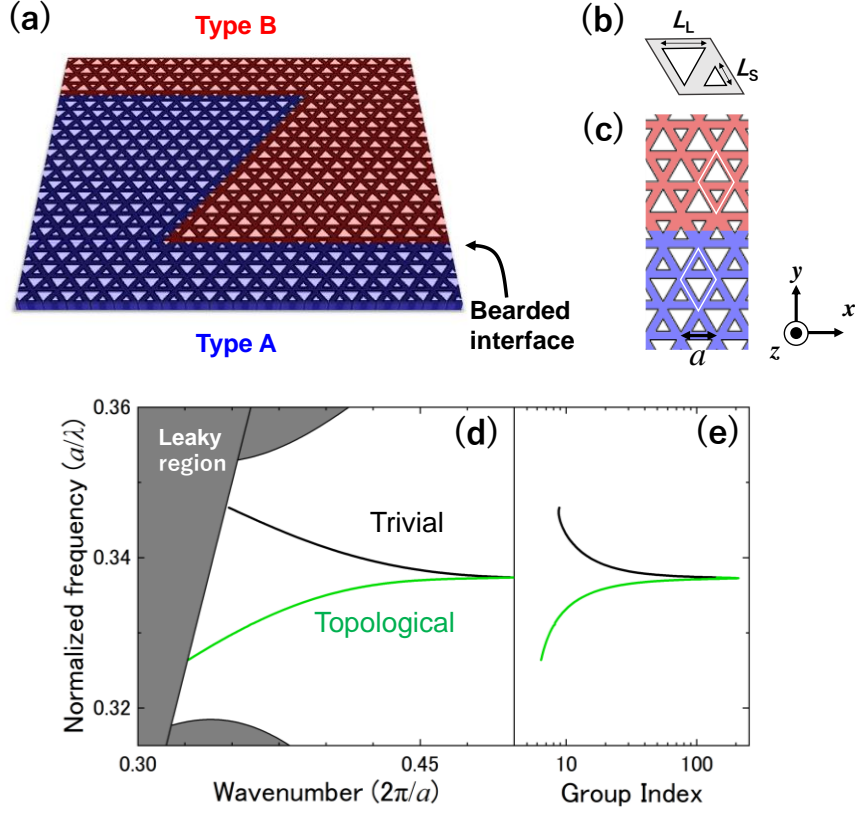


Fig. 1. Fig. 1. (a) Schematic of the investigated topological VPhC waveguide. (b) Unit cell of the VPhCs, consisting of large and small triangular air holes with respective side lengths of L_L and L_S . (c) Bearded interface formed between two topologically-distinct VPhCs. The two unit cells in each VPhCs are indicated by white solid lines. (d) Band diagram for the edge state at the bearded interface. (e) Corresponding calculated group indices for the in-gap states.

Figure 1 (a) shows a schematic of the investigated topological VPhC waveguide with a bearded interface, which has been demonstrated to exhibit slow light modes in our recent work [18,19]. Compared to previously-reported topological slow light waveguides, which utilize complex materials or structures [20–26], the VPhC slow light waveguide can be realized in a simple dielectric slab and is advantageous for coupling to solid-state emitters. The waveguide is formed at the interface between two topologically-distinct VPhCs, denoted as type A (colored in red) and type B (blue). Figure 1 (b) shows the unit cell of the VPhCs. The unit cell contains two equilateral triangle air holes with different side lengths termed L_L and L_S . In the case of $L_L = L_S$, C_{6v} point group symmetry is preserved in the system and a symmetry protected Dirac cones are supported between the

first and the second lowest frequency bands at K and K' points. On the other hand, the case of $L_L \neq L_S$ breaks spatial inversion symmetry of the system, resulting in formation of a topological bandgap between the two bands. Type A and B VPhCs coincide with each other when inverting one of them, and thus share the same band structure, but differ in their band topology. When interfacing the two VPhCs, a topological kink mode will appear within the common bandgap. Recent works have shown that the valley kink state can support robust light guiding even with sharp waveguide turns[7,8] and can significantly mitigate propagation loss and backscattering compared to conventional PhC waveguides [14,27].

Figure 1 (c) shows a bearded interface formed using the two VPhCs with large and small triangles with $L_L = 1.3a/\sqrt{3}$ and $L_S = 0.7a/\sqrt{3}$ (a is lattice constant). Figure 1 (d) shows a calculated band diagram of the VPhC waveguide with the bearded interface by the three-dimensional plane wave expansion (3D PWE) method. We consider a slab with the refractive index of $n = 3.4$ and thickness of $d = 130$ nm. We set the lattice constant a to be 310 nm. In stark contrast to conventional zigzag interfaces with fast light modes [9], the bearded interface used in this work supports two different slow light modes in the bandgap. They are degenerate at the Brillouin zone (BZ) edge due to glide plane symmetry across the interface [28]. The lower frequency mode corresponds to a topological edge state (light green curve), while the higher frequency one originates from a trivial state (black curve). The detailed discussion of the origin of these modes can be found in our previous work [18,19]. Figure 1(d) shows the corresponding group indices of the in-gap modes, showing high n_g over 100 near the BZ edge.

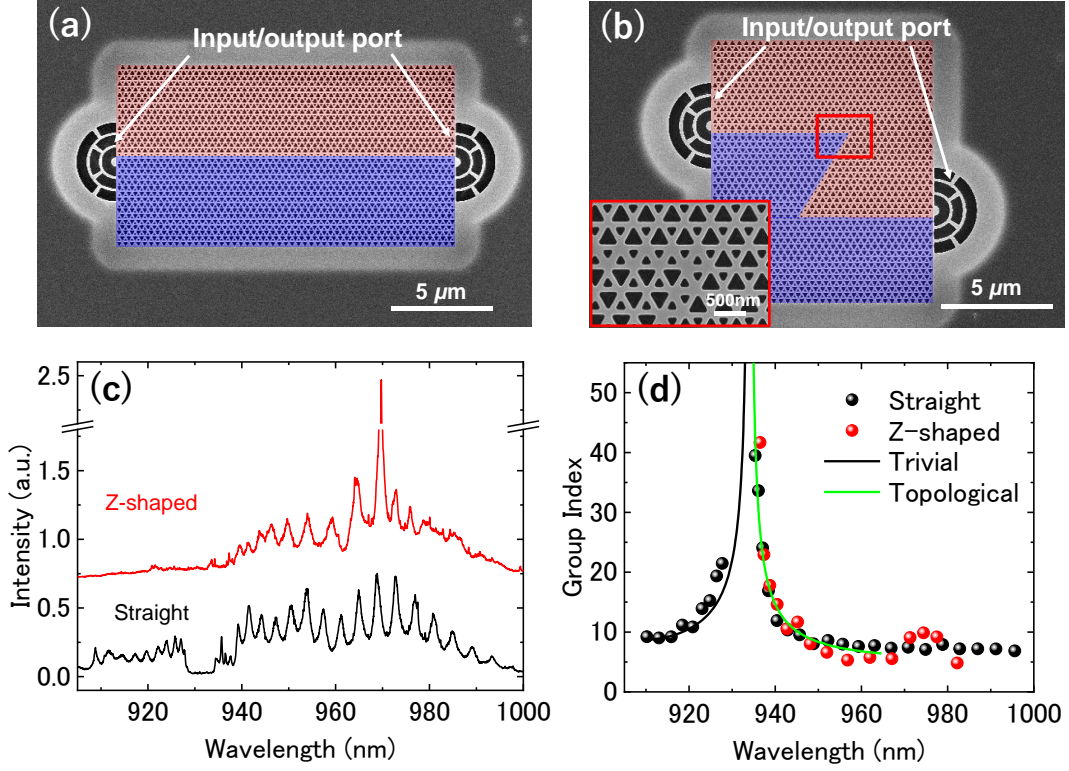


Fig. 2. SEM images of fabricated (a) straight and (b) Z-shaped waveguides. The inset image in (b) shows an enlarged view of one of the 120° bends. The blue and red colored area corresponds to type A and type B VPhCs. (c) PL spectra of straight (black) and Z-shaped (red) waveguides. (d) Group indices extracted from the measured spectra in (c). The solid curves are simulated group indices of trivial (black) and topological (light green) modes.

We fabricated straight and Z-shaped topological slow light waveguides into a 130 nm-thick GaAs slab by standard semiconductor processes based on electron beam lithography and reactive ion etching. Air-bridge structures were finally formed by removing a $1\text{ }\mu\text{m}$ -thick $\text{Al}_{0.7}\text{Ga}_{0.3}\text{As}$ sacrificial layer under the slab using hydrofluoric acid. A single layer of InAs QDs with a low areal density of $\sim 10^8\text{ cm}^{-2}$ is contained in the middle of the slab. Photoluminescence (PL) peaks of individual QDs were observed in a spectral range from 900 to 1000 nm. Figures 2 (a) and (b) show scanning electron microscope (SEM) images of one of the fabricated $52\text{ }\mu\text{m}$ -long straight and Z-shaped waveguides. Both ends of the waveguides are terminated with grating ports for light out-coupling to free space. We slightly shifted the position of the grating ports from the center of the waveguides to control the reflectance of light at the waveguide ends. For high reflective cases,

we can observe Fabry-Pérot (FP) fringes in transmission spectra, enabling the extraction of n_g of the waveguide modes [29].

First, we performed PL measurements to characterize the fabricated waveguides. The sample was placed in a liquid helium cryostat and pumped using a 775 nm pulse laser with a repetition rate of 80 MHz and a pulse duration of 1 ps. The sample temperature was kept at 60 K to clearly observe FP fringes in PL spectra. We used a 50 \times objective lens to focus the laser light onto one grating port so as to excite the QDs embedded therein. The PL signals were collected from the other grating port via the same objective lens and analyzed by a spectrometer equipped with a Si CCD camera. Figure 2(c) shows the PL spectra of both straight and Z-shaped waveguides taken at a high average excitation power of 30 μ W. We observed sharp peaks in the PL spectrum originating from FP resonances sustained by reflection at both waveguide ends. The FP fringes were observed from 910 nm to 1000 nm in the straight waveguide, while we did not see clear FP fringes in the shorter wavelength region below approximately 934 nm in the Z-shaped waveguide. The shorter wavelength band is the trivial mode with a high scattering loss when transmitting through the sharp waveguide bends. On the other hand, the longer wavelength band above 934 nm corresponds to the topological mode and thus can support robust light waveguiding even with the 120 $^\circ$ bends. These interpretations for the observations are consistent with our previous results of numerical and experimental investigations on the VPhC slow light waveguides [18,19]. From the observed FP fringes, n_g of both modes were estimated for the straight and Z-shaped waveguides, and were plotted in Fig. 2 (d). The measured n_g for both waveguides show similar values in the topological band and rapidly increase near the wavelength of \sim 934 nm. The highest n_g extracted from the measured FP fringes for the straight and Z-shaped waveguide are \sim 40 in the topological band. It is noted that we obtained higher n_g of up to \sim 56 for topological modes in a different waveguide which exhibits a clearer FP spectrum particularly near its high n_g region. These results demonstrate robust propagation of light emitted from QDs through topological slow light waveguides even under the presence of the sharp bends. The observed contrast between trivial and topological modes in PL spectra also highlights the impact of the topological protection in slow light waveguides. For the estimation of the BZ edge position of the fabricated topological waveguides, we fitted the measured n_g for 11 different samples with the same design using theoretical curves computed by the 3D PWE method (solid lines in Fig. 2 (d)). From the fitting, we deduced the wavelength of the BZ edge to be 934.0 ± 0.45 nm. The fitting curve was plotted in Fig. 2 (d) and shows a good agreement with the measured n_g . Hereafter, using the extracted n_g curve, we estimate n_g of the waveguide mode only from its wavelength of operation, after taking into account a wavelength shift depending on the operation temperature.

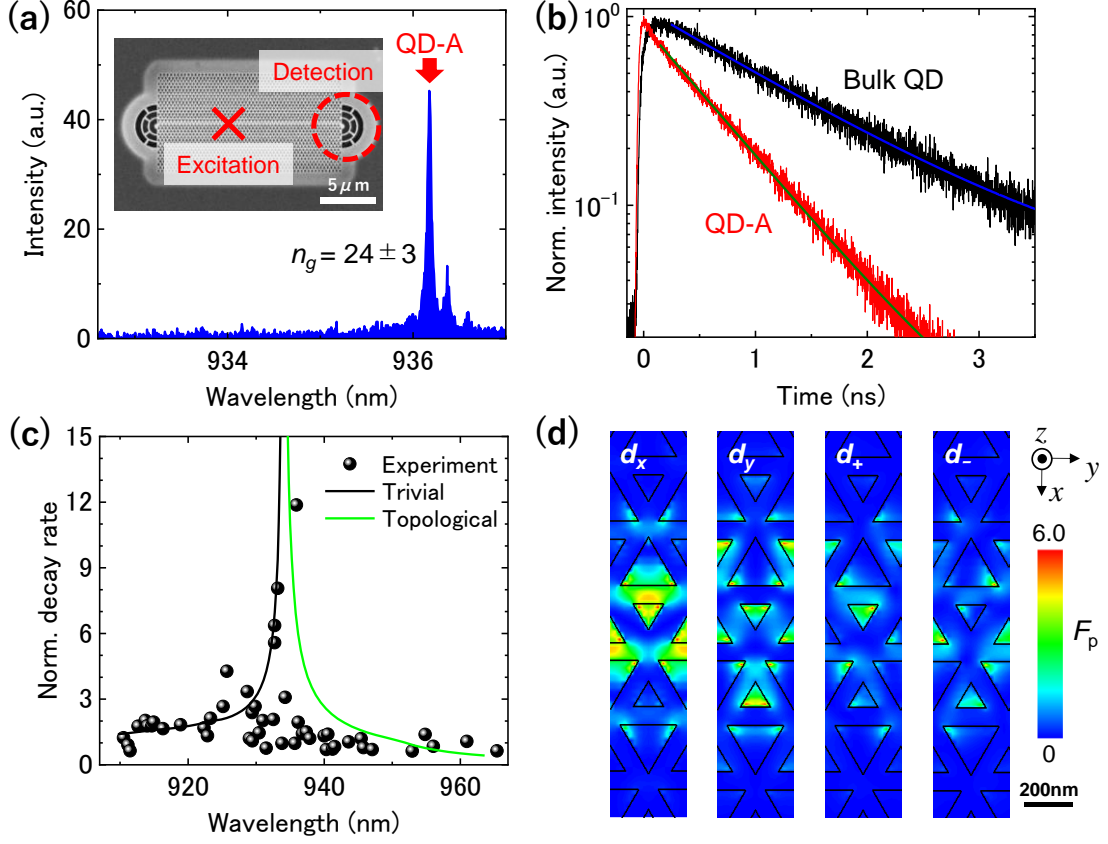


Fig. 3. (a) PL spectrum for a QD (labeled as QD-A) in a straight waveguide. Inset shows the SEM image of a waveguide, overlaid with the positions of the laser excitation (cross marker) and QD emission detection (circle maker). (b) Measured PL decay curves of QD-A (red) and a bulk QD (black). The blue and green lines are fitting curves. (c) Normalized decay rates measured for 49 QDs. The black (light green) solid line indicates calculated decay rates for the electric field (E_x) of trivial (topological) modes. (d) Distribution of calculated Purcell factor (F_p) when a slow light mode with $n_g \sim 25$ is coupled to linear dipoles (d_x or d_y) and circularly polarized dipoles (d_+ or d_-).

Next, we optically investigated single QDs in straight waveguides at 6.5K. For inspecting each single QD, we excited a QD in a waveguide and measured its PL emission from the right-side output port one by one, as depicted in the inset of Fig. 3 (a). Figure 3(a) shows an emission spectrum of a QD (labeled as QD-A) emitting at 936.17 nm. From the theoretical curve in Fig. 2 (b), the emission wavelength can be translated into a high n_g of 24 ± 3 in the topological waveguide band. We also performed time-resolved PL measurements on QD-A using a time-

correlated single-photon counting system with a superconducting single-photon detector (SSPD). The measured system time resolution was 33 ps. We selectively measured the QD emission using a spectrometer as a band-pass filter. Figure 3(b) shows the time-resolved PL spectra measured for the QD-A (red) and a QD in an unpatterned area on the same chip (black). We fitted the measured PL curves using a single exponential function convolved with the system response function. The QD lifetime for QD-A is measured to be 0.6 ns, which is approximately 2 times faster than the average lifetime for 10 QDs measured in unpatterned area (~ 1.2 ns). The observed lifetime reduction suggests that the emission rate of QD-A was enhanced by the Purcell effect in the topological slow light mode.

We also investigated wavelength dependence of QD spontaneous emission rates for 49 different QDs in 10 different straight waveguides. Figure 3(c) shows the summary of the QD emission rates normalized by that of bulk QDs. Overall, the measured decay rates tend to increase as approaching the BZ edge of ~ 934 nm, which is consistent with the trend of measured n_g . We observed the highest enhancement of ~ 12 in the topological band. We compared the measured decay rate with a theoretical model (see Supplement 1), assuming the QD dipole moment is coupled to the x component of the electric field dominant in the dielectric region (see Fig. 3 (d)). The theoretical decay rate was overlaid in Fig. 3 (c) with the same offset in the horizontal axis as that used for the theoretical curves in Fig. 2 (d). The experimental data can be well described by the theoretical curves, further confirming the Purcell-enhanced emission of the QDs in the VPhC slow light modes. Figure 3 (d) shows color maps of the Purcell factor (F_p) when a QD dipole moment is x - or y -linearly polarized ($d_x = d\hat{x}$ or $d_y = d\hat{y}$) and right- (subscript +) and left- (subscript -) circularly polarized ($d_{\pm} = d/\sqrt{2}(\hat{x} \pm i\hat{y})$, respectively). The F_p map was calculated based on the model for a topological slow light mode with $n_g \sim 25$. Whereas the maximum F_p is found inside the air holes for both E_x and E_y , there is still a certain amount of high F_p in the dielectric region, especially for E_x component. To achieve higher F_p , the precise alignment of the QD position and its polarization with respect to the local electric field could be necessary. Note that it seems difficult to simultaneously realize both good chiral and high Purcell-enhanced couplings of QDs to the current topological waveguide due to the mismatch between high chiral and high F_p points in the dielectric region (see Supplement 1), which, conversely, is suitable for chiral couplings with levitated atoms [30] and nanoparticles [31].

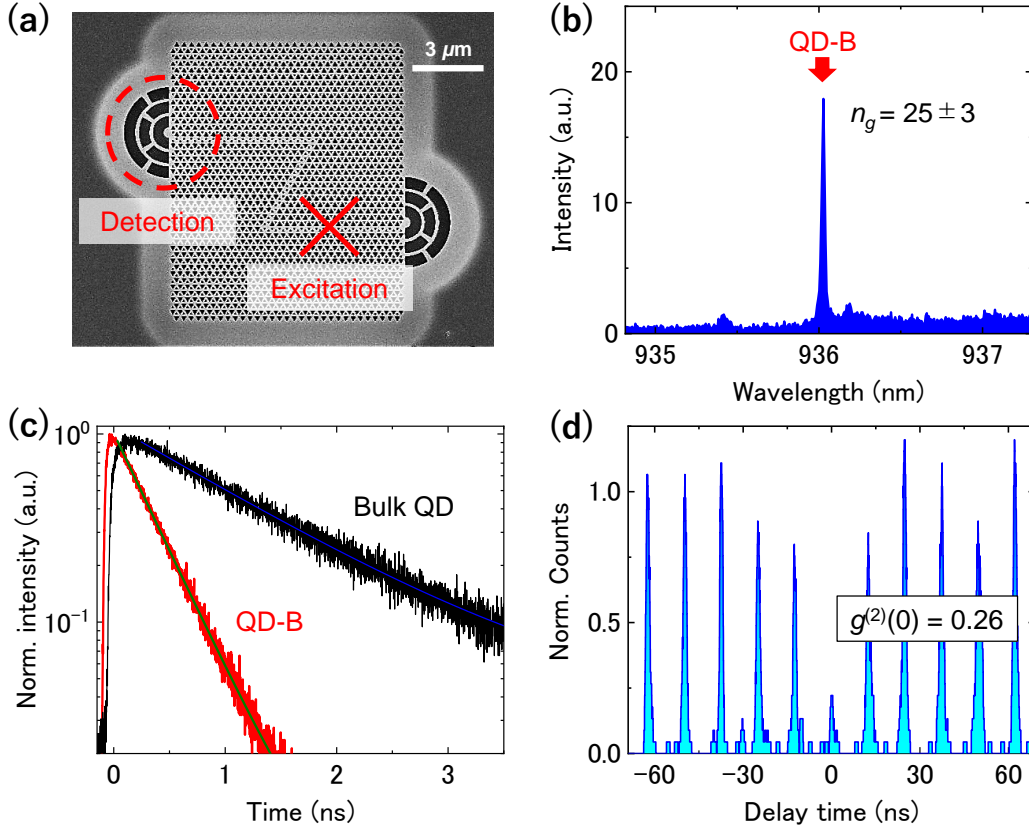


Fig. 4. (a) SEM image of a Z-shaped waveguide. The cross and circle makers indicate the positions of the excitation and detection. (b) PL spectrum of a QD (labeled as QD-B) measured at an averaged excitation power of 100 nW. (c) Time-resolved PL spectra measured for QD-B (red) and a bulk QD (black). (d) Measured second-order correlation function of QD-B.

Finally, we investigate single-photon generation from a single QD in a Z-shaped waveguide. As depicted in Fig. 4 (a), we measured QD emission from the grating port located at the top left, while pumping a QD in the waveguide located far away from the grating port. Thus, we only detect PL signals that efficiently passed through the sharp corners. Figure 4(b) shows a PL spectrum of a QD (labeled QD-B) emitting at 936.03 nm (corresponding to n_g of 25 ± 3). Figure 4 (c) shows a measured time-resolved PL spectrum for QD-B, showing a large reduction in PL lifetime due to the Purcell effect by coupling to the slow light mode. By fitting the PL curves in the same procedure described above, the PL lifetime for the QD-B was deduced to be 0.34 ns, which is more than 3 times faster than that of the bulk QD.

In order to confirm the single-photon nature of the QD emission, we performed intensity

autocorrelation measurements on QD-B using a Hanbury Brown-Twiss setup equipped with two SSPDs. Figure 4 (d) shows a measured second-order correlation function, $g^{(2)}(t)$, measured using the output port. We observed a clear antibunching behavior with $g^{(2)}(0) = 0.26$. The non-zero value at $t = 0$ could be attributed to background emission from the FP fringes supplied by other QDs inside the waveguide. These results demonstrate Purcell-enhanced single-photon generation from a single QD in a topological slow light waveguide and its efficient propagation even under the presence of sharp bends.

In summary, we have demonstrated QD-based single-photon sources embedded in topological slow light VPhC waveguides. We observed a large reduction in PL lifetime of a single QD by a factor of up to ~ 12 due to the Purcell effect in the topological slow light modes. In the slow light regime with a high n_g of ~ 25 , we demonstrated Purcell-enhanced single-photon generation from a QD and its robust propagation even under the presence of sharp waveguide bends. These results will be of importance for the development of topologically-protected IQPCs with robust and high-performance single-photon sources.

ACKNOWLEDGMENTS

We thank Prof. M. Lončar, M. Nishioka, S. Ishida, T. Yamaguchi and W. Lin for their technical support and helpful discussions. This work was supported by JSPS KAKENHI Grant-in-Aid for Specially Promoted Research (15H05700); KAKENHI (17H06138, 18J13565, 19K05300); JST-CREST (JPMJCR19T1); Asahi Glass Foundation; New Energy and Industrial Technology Development Organization (NEDO); JSPS Overseas Research Fellowships (202160592).

REFERENCES

1. T. Baba, *Nat. Photonics* **2**, 465 (2008).
2. A. Javadi, I. Söllner, M. Arcari, S.L. Hansen, L. Midolo, S. Mahmoodian, G. Kiršanskė, T. Pregmolato, E.H. Lee, J.D. Song, S. Stobbe, and P. Lodahl, *Nat. Commun.* **6**, 8655 (2015).
3. I. Söllner, S. Mahmoodian, S.L. Hansen, L. Midolo, A. Javadi, G. Kiršanskė, T. Pregmolato, H. El-Ella, E.H. Lee, J.D. Song, S. Stobbe, and P. Lodahl, *Nat. Nanotechnol.* **10**, 775 (2015).
4. S. Assefa, S.J. McNab, and Y.A. Vlasov, *Opt. Lett.* **31**, 745 (2006).
5. L. O’Faolain, S.A. Schulz, D.M. Beggs, T.P. White, M. Spasenović, L. Kuipers, F. Morichetti, A. Melloni, S. Mazoyer, J.P. Hugonin, P. Lalanne, and T.F. Krauss, *Opt. Express* **18**, 27627 (2010).
6. T. Ozawa, H.M. Price, A. Amo, N. Goldman, L. Lu, M.C. Rechtsman, and D. Schuster, *Rev. Mod. Phys.* **91**, 15006 (2019).
7. M.I. Shalaev, W. Walasik, A. Tsukernik, Y. Xu, and N.M. Litchinitser, *Nat. Nanotechnol.* **14**, 31 (2019).
8. X.-T. He, E.-T. Liang, J.-J. Yuan, H.-Y. Qiu, X.-D. Chen, F.-L. Zhao, and J.-W. Dong, *Nat. Commun.* **10**, 872 (2019).
9. T. Yamaguchi, Y. Ota, R. Katsumi, K. Watanabe, S. Ishida, A. Osada, Y. Arakawa, and S. Iwamoto, *Appl. Phys. Express* **12**, 062005 (2019).
10. J. Ma, X. Xi, and X. Sun, *Laser Photon. Rev.* **13**, 1900087 (2019).
11. M. Jalali Mehrabad, A.P. Foster, R. Dost, E. Clarke, P.K. Patil, A.M. Fox, M.S. Skolnick, and L.R. Wilson, *Optica* **7**, 1690 (2020).
12. W. Noh, H. Nasari, H.-M. Kim, Q. Le-Van, Z. Jia, C. Huang, and B. Kanté, *Opt. Lett.* **45**, 4108 (2020).
13. Y. Zeng, U. Chattopadhyay, B. Zhu, B. Qiang, J. Li, Y. Jin, L. Li, A.G. Davies, E.H. Linfield, B. Zhang, Y. Chong, and Q.J. Wang, *Nature* **578**, 246 (2020).
14. S. Arora, T. Bauer, R. Barczyk, E. Verhagen, and L. Kuipers, *Light Sci. Appl.* **10**, 9 (2021).
15. X. Xie, S. Yan, J. Dang, J. Yang, S. Xiao, Y. Wang, S. Shi, L. Yang, D. Dai, Y. Yuan, N. Luo, T. Cui, G. Chi, Z. Zuo, B.-B. Li, C. Wang, and X. Xu, *Phys. Rev. Appl.* **16**, 014036 (2021).
16. S. Barik, A. Karasahin, S. Mittal, E. Waks, and M. Hafezi, *Phys. Rev. B* **101**, 205303 (2020).
17. S. Barik, A. Karasahin, C. Flower, T. Cai, H. Miyake, W. DeGottardi, M. Hafezi, and E. Waks, *Science* **359**, 666 (2018).
18. H. Yoshimi, T. Yamaguchi, Y. Ota, Y. Arakawa, and S. Iwamoto, *Opt. Lett.* **45**, 2648 (2020).
19. H. Yoshimi, T. Yamaguchi, R. Katsumi, Y. Ota, Y. Arakawa, and S. Iwamoto, *Opt. Express*

- 29, 13441 (2021).
20. Y. Yang, Y. Poo, R.X. Wu, Y. Gu, and P. Chen, Appl. Phys. Lett. **102**, (2013).
21. X.-D. Chen, Z. Deng, W. Chen, J. Wang, and J. Dong, Phys. Rev. B **92**, 014210 (2015).
22. S.A. Hassani Gangaraj and F. Monticone, Phys. Rev. Lett. **121**, 093901 (2018).
23. J.-F. Chen, W. Liang, and Z.-Y. Li, Photonics Res. **7**, 1075 (2019).
24. J. Guglielmon and M.C. Rechtsman, Phys. Rev. Lett. **122**, 153904 (2019).
25. J. Chen, W. Liang, and Z.-Y. Li, Opt. Lett. **45**, 4964 (2020).
26. Y.-H. Chang, R.A.R. Robles, V.C. Silalahi, C.-S. Wu, G. Wang, G. Marcucci, L. Piloizzi, C. Conti, R.-K. Lee, and W. Kuo, ArXiv:2004.09282 (2020).
27. G. Arregui, J. Gomis-Bresco, C.M. Sotomayor-Torres, and P.D. Garcia, Phys. Rev. Lett. **126**, 027403 (2021).
28. A. Mock, L. Lu, and J. O'Brien, Phys. Rev. B **81**, 155115 (2010).
29. M. Notomi, K. Yamada, A. Shinya, J. Takahashi, C. Takahashi, and I. Yokohama, Phys. Rev. Lett. **87**, 253902 (2001).
30. I. Shomroni, S. Rosenblum, Y. Lovsky, O. Bechler, G. Guendelman, and B. Dayan, Science **345**, 903 (2014).
31. J. Petersen, J. Volz, and A. Rauschenbeutel, Science **346**, 67 (2014).

Topologically-protected single-photon sources in topological slow light photonic crystal waveguides: supplemental document

Kazuhiro Kuruma,^{1, 2, 3,*} Hironobu Yoshimi,^{1,2} Yasutomo Ota,^{4,5} Ryota Katsumi,^{1,2}
Masahiro Kakuda,⁵ Yasuhiko Arakawa,⁵ and Satoshi Iwamoto^{1,2,5}

¹ *Research Center for Advanced Science and Technology, The University of Tokyo, 4-6-
Komaba, Meguro-ku, Tokyo 153-8505, Japan*

² *Institute of Industrial Science, The University of Tokyo, 4-6-1 Komaba, Meguro-ku,
Tokyo 153-8505, Japan*

³ *John A. Paulson School of Engineering and Applied Sciences, Harvard University,
Cambridge, MA 02138, USA*

⁴ *Department of Applied Physics and Physico-Informatics, Keio University, 3-14-1
Hiyoshi, Kohoku-ku, Yokohama, Kanagawa 223-8522, Japan*

⁵ *Institute of Nano Quantum Information Electronics, The University of Tokyo, 4-6-1
Komaba, Meguro-ku, Tokyo 153-8505, Japan*

*Corresponding author: kuruma@iis.u-tokyo.ac.jp

1. Calculation of QD emission decay rates into waveguides

In this calculation, we consider a GaAs-based two-dimensional photonic crystal waveguide shown in Fig. 1 (c) of the main text. The refractive index n of the GaAs slab is 3.4. The waveguide supports a transverse electric (TE) mode with a group index n_g . We assume QDs as point dipole sources (dipole approximation). The QD emission decay rate into a waveguide mode Γ_{wg} , normalized to the decay rate in bulk Γ_0 is given by [1]

$$\frac{\Gamma_{wg}}{\Gamma_0} = \frac{3}{4\pi} \frac{(\lambda/n)^2}{S_{eff}} \frac{n_g}{n} \frac{|\mathbf{E}(\mathbf{r}) \cdot \mathbf{d}|^2}{|\mathbf{d}|^2 |\mathbf{E}_{max}|^2} \quad (\text{S1})$$

where λ is the vacuum wavelength and \mathbf{d} is the electric dipole moment of the QD. The effective mode area is defined as $S_{eff} = \iint n(\mathbf{r})^2 |\mathbf{E}(\mathbf{r})|^2 d^2\mathbf{r} / \max [n(\mathbf{r})^2 |\mathbf{E}(\mathbf{r})|^2]$. Here, $\mathbf{E}(\mathbf{r})$ represents local electric field at a position \mathbf{r} in the waveguide. The electric field of the waveguide modes was calculated by the 3D plane wave expansion method. We assumed that the QD dipole is primarily coupled to the electric field towards the wave propagation direction (E_x). Since the QDs exist only in the GaAs slab, the maximum possible Γ_{wg} s were calculated using the maximum field intensity within the dielectric region. The calculated Γ_{wg} s for each waveguide mode plotted in Fig. 3 (c) in the main text have a constant offset of typical decay rate of InAs QDs in 2D photonic bandgap $\Gamma_{PC} \sim 0.1\Gamma_0$ [2]. To obtain the profile of theoretical Purcell factors (F_p) in the waveguide for x or y -linear dipoles (\mathbf{d}_x or \mathbf{d}_y), and right- or left- circularly polarized dipoles (\mathbf{d}_+ or \mathbf{d}_-), we calculated F_p based on eq (S1).

2. Mode map of Purcell factor (F_p) and chiral spatial map for the topological waveguide with a beaded interface

Figure S1 (a) shows a calculated F_p distribution for the case considering a right- or left-circularly polarized (\mathbf{d}_+ or \mathbf{d}_-) dipoles. $\sigma^+(\sigma^-)$ corresponds to the dipole moment of $\mathbf{d}_+(\mathbf{d}_-)$. A corresponding spatial map of normalized Stokes S_3 parameter, for a topological mode with a group index (n_g) of 25 is shown in Fig. S1 (b). Normalized S_3 was calculated using the following equation:

$$S_3 = \frac{-2 \operatorname{Im}(E_x E_y^*)}{|E_x|^2 + |E_y|^2} \quad (\text{S2})$$

Here, E_x and E_y are the electric field of x and y components in waveguide. The locations at which $|S_3|$ approaches 1 will exhibit strong chiral coupling with a circularly polarized QD emission.

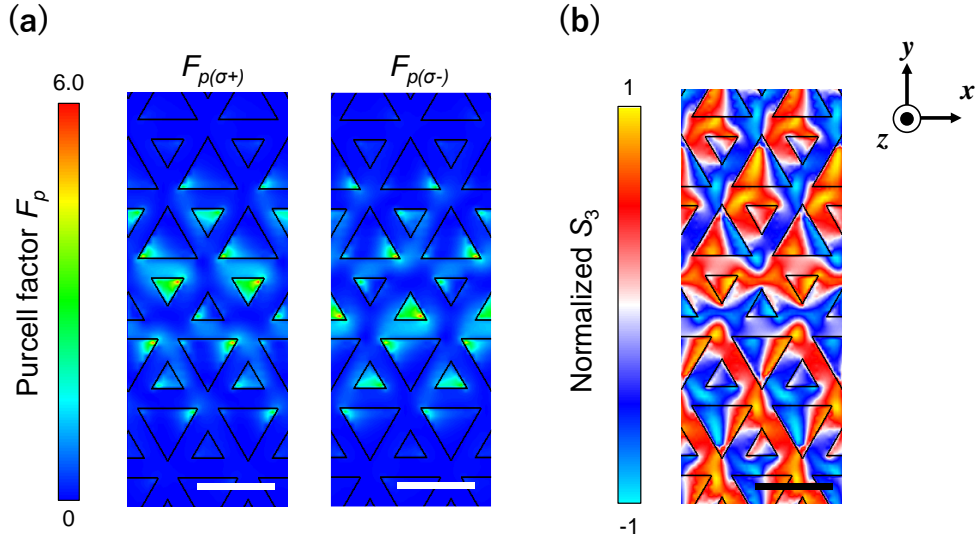


Fig. S1. Mode profile of Purcell factor for σ^+ and σ^- dipoles (a), and of normalized S_3 parameter (b) for a bearded topological waveguide with n_g of 25. The white and black scale bars in (a) and (b) are 300 nm.

References

1. Q. Quan, I. Bulu, and M. Lončar, "Broadband waveguide QED system on a chip," Phys. Rev. A **80**, 011810 (2009).
2. Q. Wang, S. Stobbe, and P. Lodahl, "Mapping the Local Density of Optical States of a Photonic Crystal with Single Quantum Dots," Phys. Rev. Lett. **107**, 167404 (2011).